Proteomic Analysis of the Soluble Fraction from Human Corneal Fibroblasts with Reference to Ocular Transparency*

Henrik Karring‡§, Ida B. Thøgersen§, Gordon K. Klintworth¶, Jan J. Enghild§, and Torben Møller-Pedersen‡‖

The transparent corneal stroma contains a population of corneal fibroblasts termed keratocytes, which are interspersed between the collagen lamellae. Under normal conditions, the keratocytes are quiescent and transparent. However, after corneal injury the keratocytes become activated and transform into backscattering wound-healing fibroblasts resulting in corneal opacification. At present, the most popular hypothesis suggests that particular abundant water-soluble proteins called enzyme-crystallins are involved in maintaining corneal cellular transparency. Specifically, corneal haze development is thought to be related to low levels of cytoplasmic enzyme-crystallins in reflective corneal fibroblasts. To further investigate this hypothesis, we have used a proteomic approach to identify the most abundant water-soluble proteins in serum-cultured human corneal fibroblasts that represent an *in vitro* model of the reflective wound-healing keratocyte phenotype. Densitometry of one-dimensional gels revealed that no single protein isoform exceeded 5% of the total water-soluble protein fraction, which is the qualifying property of a corneal enzyme-crystallin according to the current definition. This result indicates that wound-healing corneal fibroblasts do not contain enzyme-crystallins. A total of 254 protein identifications from two-dimensional gels were performed representing 118 distinct proteins. Proteins protecting against oxidative stress and protein misfolding were prominent, suggesting that these processes may participate in the generation of cytoplasmic light-scattering from corneal fibroblasts. *Molecular & Cellular Proteomics 3:660–674, 2004.*

The cornea, the only transparent connective tissue of the body, is responsible for ~70% of the total refractive power of visible light in the eye. The corneal stroma (thickness ~450 μm) mainly consists of collagen lamellae formed by uniform fibrils composed of type I, III, and V collagen (1, 2). The uniform diameter (~30 nm) and regular spacing of the collagen fibrils (~60 nm between the centers) lead to destructive interference of light except in the forward direction and thus optical transparency of the extracellular matrix of the cornea (3, 4). The stroma also contains multiple layers of quiescent corneal fibroblasts, termed keratocytes, which are interspersed between the collagen lamellae. Under normal conditions, the quiescent keratocytes are transparent except for the nuclei when studied *in vivo* using scanning slit specular microscopy (5), slit-lamp biomicroscopy, or *in vivo* confocal microscopy (6). This stealth-like invisibility indicates that the refractive index of the keratocyte cytoplasm and cellular processes is similar to that of the extracellular matrix of the corneal stroma (6).

The keratocytes have a dynamic potential for proliferation and transformation. Thus, after injury of the cornea such as excimer laser keratectomy for the treatment of myopia, the keratocytes transform into spindle-shaped fibroblastic cells (7, 8). The corneal fibroblasts repopulate the damaged region by migration and proliferation and deposit disordered and nontransparent matrix components (9–11). The damaged stroma is then remodelled through continuous degradation and synthesis of the extracellular matrix to recreate the highly ordered collagen structure (11, 12). In the latest phase of the wound-healing process, the corneal fibroblasts undergo a phenotype change into myofibroblasts, which are responsible for wound contraction (13–15). The wound-healing process reduces the optical clarity of the cornea due to an increase in the light-scattering from the cell bodies of the corneal fibroblasts compared with that of keratocytes (7, 8, 16, 17). These results suggest that development of corneal cellular haze during wound-healing is caused in part by an increase in the backscatter of light from the cytoplasm of the stromal cells.

The maintenance of ocular transparency and the development of opacities have been studied intensively in the ocular lens. The α- and β/γ-crystallins are the major water-soluble proteins of all vertebrate ocular lenses and are critical for the optical properties and transparency of this tissue. The α-crystallins are members of the small heat shock protein family and have chaperone-like activity preventing the aggregation of proteins (18, 19). The β/γ-crystallins are related to microbial

oxidative stress proteins (20) and have been implicated in the development of cataracts (21). The high concentration and oligomeric complex formations of the α- and β/γ-crystallins are believed to give the ocular lens its refractive index and optical properties through short-range spatial orders (22).

Several studies of various vertebrates and invertebrates have shown taxon-specific accumulations of water-soluble proteins in the lens and epithelial cells of the cornea. The abundant taxon-specific proteins in the lens and cornea are often similar or identical to metabolic enzymes and, therefore, termed enzyme-crystallins. Most mammals accumulate aldehyde dehydrogenase 3 (ALDH3)[1] in the corneal epithelium (23–26). Transketolase (TKT) is a major protein in the mouse and human corneal epithelium (27), and α-enolase is relatively abundant in human, mouse, and chicken corneas (26). Isocitrate dehydrogenase is overexpressed in the bovine corneal epithelium (28), while peptidyl-prolyl *cis-trans* isomerase and argininosuccinate lyase are found at high concentrations in the corneal epithelium of chicken (26). Glutathione *S*-transferase-related *S*-crystallin is abundant in squid cornea (26), while zebrafish accumulates gelsolin and actin in the corneal epithelium (29). It has been suggested that proteins present at a concentration exceeding 5% of the total water-soluble protein content of corneal cells should be defined as enzyme-crystallins (30). The function of the corneal enzyme-crystallins is not clear, but it has been suggested that they serve catalytic as well as structural roles reminiscent to the α- and β/γ-crystallins in the lens and thereby contribute to the transparency and optical properties of the corneal cells.

TKT and ALDH1 are abundant proteins in rabbit keratocytes (17). These two proteins comprise about 30% of the total water-soluble protein content in freshly isolated keratocytes from normal rabbit corneas, but are reduced to less than 15% in light-scattering corneal fibroblasts (17). These results indicate an apparent correlation between cellular transparency and the levels of enzyme-crystallins in stromal cells of the cornea. However, ALDH3A1-deficient mice (31) and TKT^{+/−} (32) mice show no corneal phenotype, indicating that the enzyme-crystallins are not required for corneal transparency. Other studies have indicated that the abundant water-soluble enzyme-crystallins protect the cornea against ultraviolet (UV)-induced oxidative injury. Thus, isocitrate dehydrogenase prevents lipid peroxidation and oxidative DNA damage (33), while ALDH3A1 detoxifies the cellular environment by removing toxic aldehydes generated by lipid peroxidation (34, 35). In addition, ALDH3A1 may function as a UV-light filter in the cornea by directly absorbing UV radiation (36). However, de-

spite the various suggestions concerning the roles of the abundant water-soluble proteins in the corneal, it is reasonable to believe that maintenance of corneal transparency and the development of cellular haze are dependent on the protein expression profile.

In the present study, the soluble proteome of cultured human corneal fibroblasts was analyzed by one-dimensional (1D) and two-dimensional (2D) PAGE, and 118 of the most abundant water-soluble proteins were identified by matrix-assisted laser desorption/ionization (MALDI) mass spectrometry (MS) or MALDI quadrupole time-of-flight (TOF) tandem mass spectrometry (MS/MS). The identified proteins are involved in processes such as protein folding and degradation, cell proliferation, differentiation, and apoptosis, metabolism, cytoskeleton organization and cell motility, protection against oxidative stress, signal transduction, and secretion of proteins. Based on the identified proteins, we propose that oxidative stress may lead to protein unfolding that may participate in the enhanced backscatter of light from corneal fibroblasts. Aggregation of irreversible oxidized proteins is known to opacify the crystalline lens. Thus, it is possible that development of corneal cellular haze during wound-healing is somehow reminiscent to the formation of an oxidative stress-induced opacity in the crystalline lens.

EXPERIMENTAL PROCEDURES

Cell Culture—Four human donor corneas (males of 39 and 51 years old and females of 66 and 73 years old) were obtained from the Danish Cornea Bank, Aarhus University Hospital, and dissected in Hanks' buffered saline solution (HBSS; Life Technologies, Inc., Grand Island, NY). After removing the Descemet's membrane-endothelial complex and the epithelium, the central stroma was punched from the endothelial side using a 7-mm trephine. The stromal buttons were cut into 1-mm³ pieces and washed three times in 1 ml of HBSS before being used for explants in 40-ml cell-culture flasks (Nunc, Roskilde, Denmark).

The corneal fibroblasts were cultured at 37 °C in a 5% CO_2-humidified incubator in Dulbecco's modified Eagle's medium/NUT MIX F-12 (HAM) medium (Life Technologies, Inc.) containing 10% fetal bovine serum (Life Technologies, Inc.), 100 U/ml penicillin, 100 μg/ml streptomycin (Life Technologies, Inc.), and 0.25 μg/ml fungizone (amphotericin B) (Life Technologies, Inc.). When the cultures had multiplied to confluence, the cells were trypsinized by 0.25% (w/v) trypsin/1 mM EDTA mixture (Life Technologies, Inc.) and transferred to a 250-ml cell-culture flask (first passage). Subsequently, confluent cultures were split in 1:4 and cells from the third passage were washed in phosphate-buffered saline (PBS) Dulbecco's (Life Technologies, Inc.) before harvested by scraping using a cell scraper in PBS Dulbecco's. Cells were spun down at 1,000 × g for 10 min at 25 °C and washed thoroughly three times in the same buffer. After washing and centrifugation, the corneal fibroblasts were resuspended in 0.1 × PBS Dulbecco's diluted in water and containing 2 mM 1,10-phenanthroline (Sigma, St. Louis, MO), 40 μM *trans*-epoxysuccinyl-L-leucylamido(4-guanidino)-butane (E-64) (Sigma), and 2 mM pefabloc SC (Fluka, Buchs, Switzerland). Cells were lysed by sonication on ice, and the soluble fraction was isolated by centrifugation at 33,000 × g for 15 min at 4 °C and stored at −80 °C.

1D and 2D PAGE—For 1D SDS-PAGE, the soluble fraction of the corneal fibroblasts was mixed with SDS sample buffer containing 1

---

[1] The abbreviations used are: aa, amino acid; ALDH, aldehyde dehydrogenase; 1D, one-dimensional; 2D, two-dimensional; DTT, dithiothreitol; ER, endoplasmic reticulum; IL, interleukin; MALDI, matrix-assisted laser desorption/ionization; MS, mass spectrometry; MS/MS, tandem mass spectrometry; PBS, phosphate-buffered saline; ROS, reactive oxygen species; TOF, time-of-flight; TKT, transketolase; Ub, ubiquitin; UV, ultraviolet.

mM dithiothreitol (DTT) and run in 5–15% gradient gels using the glycine, 2-amino-2-methyl-1,3-propanediol/HCl system described by Bury (37). Gels were Coomassie blue stained, and densitometry was performed on three samples.

For 2D PAGE, the soluble fraction of the corneal fibroblasts was mixed with sample buffer (5 M urea, 2 M thiourea, 2% (w/v) 3-[(3-cholamidopropyl)-dimethylammonio]-1-propanesulfonate (Chaps) (Sigma), 2% (w/v) N-decyl-N,N-dimethyl-3-ammonio-1-propanesulfonate (SB3–10) (Sigma), 10 mM DTT, 2 mM EDTA, 2 mM 1,10-phenanthroline, 40 μM E-64, 2 mM pefabloc SC, and 0.5% (v/v) carrier ampholytes (Amersham Biosciences, Piscataway, NJ) of pH 4–7 or 6–11 in accordance with the immobilized pH gradients (38, 39) to a final protein concentration of 0.5–1 mg/ml and incubated for 1 h at 25 °C under rotation. Bromphenol blue was added to the samples to a final concentration of 10 μg/ml, and insoluble material was removed by centrifugation at 33,000 × g for 30 min at 25 °C. The solubilized sample (350 μl) was loaded onto 18-cm Immobiline DryStrips (Amersham Biosciences) with pH ranges of 4.5–5.5, 5.5–6.7, 4–7, or 6–9 and covered with DryStrip Cover Fluid (Amersham Biosciences). After incubation for 12–18 h at 25 °C, the isoelectric focusing was performed for 16–18 h using the IPGphor System I (Amersham Biosciences) and according to the protocol of Görg et al. (40). Proteins were focused in the first electrophoresis dimension for about 124 kVh. The proteins were reduced and alkylated by incubating the immobilized pH gradient strips in 10 ml of reduction buffer (6 M urea, 50 mM Tris-HCl (pH 8.8), 30% (v/v) glycerol, 2% (v/v) SDS, and 6.5 mM DTT) at 25 °C for 15 min under rotation and in 10 ml of alkylation buffer (6 M urea, 50 mM Tris-HCl (pH 8.8), 30% (v/v) glycerol, 2% (v/v) SDS, and 10 mM iodoacetamide) at 25 °C for 15 min under rotation, respectively.

For the second-dimensional electrophoresis, the strips were transferred to 18 × 23.4-cm SDS-polyacrylamide gels (12.5%), covered with 0.5% agarose, and run in a Hoefer DALT™ tank (Amersham Biosciences) for 6 h at about 17,000 W per gel at 20 °C in running buffer containing 25 mM Tris, 192 mM glycine, and 0.1% (w/v) SDS. The gels were fixed overnight, and proteins were visualized by silver-staining as described for MS analysis (41). Gels were scanned and stored in 5% (v/v) acetic acid at 6 °C.

Sample Preparation for MS Analysis—2D gel spots of interest were excised and washed in 0.5 ml of water and incubated two times in 0.1 ml of 50% (v/v) acetonitrile for 15 min. The gel plugs were dehydrated by incubation in 50 μl of acetonitrile for 15 min and equilibrated in 50 μl of 0.1 M NH$_4$HCO$_3$ for 5 min before 50 μl of acetonitrile was added, and the samples were incubated for 15 min. After removal of the supernatant, the gel plugs were lyophilized in a speed-vac for 10 min. The in-gel digestion was performed by adding 5 μl of 50 mM NH$_4$HCO$_3$ containing 25 μg/ml sequencing-grade modified trypsin from porcine (Promega, Madison, WI) followed by incubation at 20 °C for 5 min. NH$_4$HCO$_3$ (15 μl of 50 mM) was added to the samples followed by incubation at 37 °C for 16–18 h.

For MALDI-MS analysis, the resulting tryptic-digested peptides were isolated using ZipTip P10 pipette tips (Millipore, Bedford, MA) and spotted onto the MALDI sample target using 0.5 μl of matrix solution containing 70% (v/v) acetonitrile, 0.03% (v/v) trifluoroacetic acid (protein sequencer grade), and 0.4% (w/v) recrystallised α-cyano-4-hydroxy-cinnamic acid (Sigma).

Protein Identification by MALDI-MS or MS/MS—MALDI-TOF MS or MS/MS data was acquired using a Q-Tof Ultima Global instrument (Micromass/Waters Corp., Manchester, United Kingdom). The mass spectrometer was calibrated over the range m/z 50–3000 using polyethylene glycol mixture (1.7 mg/ml PEG200, PEG400, PEG600, PEG1000, and PEG2000, and 0.28 mg/ml NaI in 50% (v/v) acetonitrile). Each spectrum was calibrated using glu-fibrinopeptide B (molecular weight = 1570.6774) (Sigma) as lock mass.

For peptide fingerprinting, mass spectra were acquired in the positive-ion mode over the range 800–3000 m/z. The mass list of peptides were used to search the Swiss-Prot/TrEMBL (42) or NCBInr protein databases on a local Mascot server using search engine Mascot software (Matrix Sciences, London, United Kingdom) (43). The searches were performed with a peptide mass tolerance of 50 ppm, carbamidomethyl modification of cystein residues, and allowed a single missed tryptic cleavage. Only significant hits as defined by Mascot probability analysis and with at least five matches of peptide masses were accepted. Usually, the peptide mass accuracy was within 10 ppm.

Tandem mass spectrometry was performed for proteins not identified by peptide fingerprinting. An abundant MS precursor ion was selected and the MS/MS data were acquired. Argon was used as a collision gas, and the collision energy required for fragmentation ranged from 50 to 120 V depending on the peptide mass. The MS/MS data were calibrated by fixing the MS precursor ion to its m/z obtained from MS. The resulting mass list of fragmented peptides was used to search the protein databases using the search engine Mascot software (Matrix Sciences) (43). The searches were performed with a peptide mass tolerance of 2 Da, MS/MS ion mass tolerance of 0.8 Da, carbamidomethyl modification of cystein residues, and up to one missed cleavage. For all identifications, human protein databases were used.

RESULTS

1D PAGE and Quantification by Densitometry—When transparent keratocytes are exposed to fetal bovine serum, they transform into the reflective phenotype characterized by a spindle-shaped morphology and a fibroblastic cytoskeleton organization (44, 45). Thus, cultured human corneal fibroblasts of the third passage (Fig. 1A) were used as an *in vitro* model system for the study of the corneal fibroblast soluble proteome. For initial analysis, the soluble fraction was analyzed by 1D PAGE. Quantification by densitometry of 1D gels showed that no single protein isoform exceeded 2.5% of the total amount of protein in the soluble fraction. Identification of the four most intensive bands revealed that the most abundant proteins were actin, two different vimentin isoforms, and annexin A2. Thus, actin (~47 kDa) makes up 2.1 ± 0.2% of the soluble protein content, while two vimentin isoforms of ~59 and ~51.3 kDa makes up 1.5 ± 0.1 and 1.1 ± 0.1%, respectively. Annexin A2 (~38 kDa) accounts for 1.0 ± 0.2% of the total protein in the soluble fraction (Fig. 1B).

Proteome Study Using 2D PAGE—The soluble proteome of the corneal fibroblasts was further analyzed by 2D PAGE using pH gradients 4–7 (Fig. 2A), 6–9 (Fig. 2B), 4.5–5.5 (Fig. 2C), and 5.5–6.7 (Fig. 2D). No obvious differences in the protein expression profiles among the donors were observed. All together, 254 gel spots were analyzed and identified by MALDI-MS or MS/MS. Thus, all spots indicated in Fig. 2 were identified by mass spectrometry. The identified proteins represented 118 distinct proteins, which were categorized according to function and cellular localization as reported in the current literature (Table I). In cases where it was obvious that the same spot had been analyzed on different gels, the spots were given the same spot ID (Fig. 2, A–D). Most of the identified proteins are involved in processes such as protein folding and degradation, cell proliferation, differentiation, and apo-
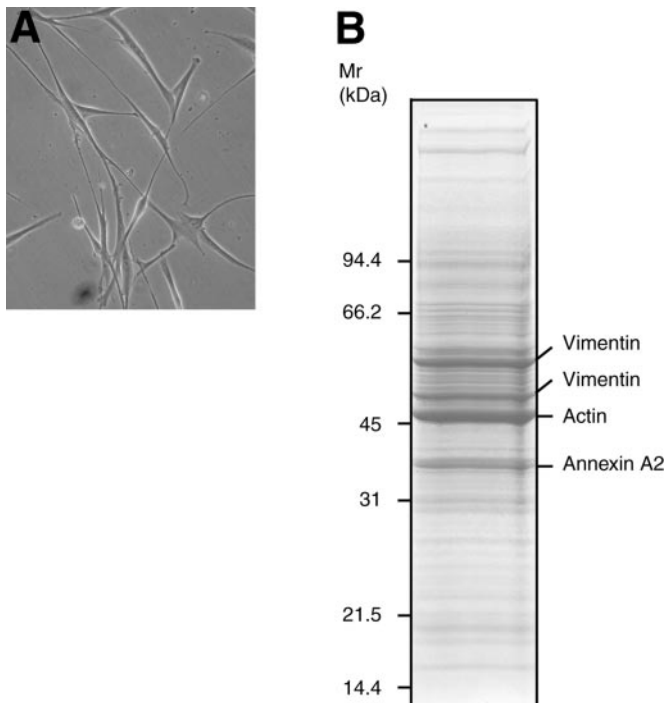
FIG. 1. **Cultured corneal fibroblasts and 1D SDS-PAGE.** *A*, spindle-shaped human corneal fibroblasts cultured in 10% fetal bovine serum. *B*, 1D SDS gel of soluble fraction from human corneal fibroblasts. The gel is Coommasie blue stained, and the identities of the four most intense bands are indicated.

ptosis, metabolism, cytoskeleton organization and cell motility, protection against oxidative stress, signal transduction, and secretion of proteins. Thus, 32 of the identified proteins are involved in protein folding and degradation (F), 24 in cell proliferation, differentiation, and apoptosis (P), 23 in metabolism (M), 21 are associated with cytoskeleton organization and cell motility (C), 17 in redox regulation and oxidative stress defense (O), 13 in signal transduction (L), 11 in the secretory pathway (S), and the rest of the proteins are involved in other functions such as cell immune defense (I), protein synthesis (Y), transcription, splicing, ion transport, and osmotic regulation (T) (Table I).

Among the identified proteins, one spot (spot 235) appeared to be a hypothetical protein (accession number Q9BTK7, TrEMBL entry) for which there is no experimental evidence that it is expressed *in vivo*. A protein-protein BLAST search revealed high identity to the C19orf10 protein (AAH03639 and NP_061980) (E-value 6e-77), other hypothetical proteins, and high homology to mouse interleukine-25 (IL-25/SF20) (NP_543027) (E-value 6e-66). The C19orf10 protein has a full-length of 173 aa, a theoretical pI ~6.2, and theoretical molecular mass ~18.8 kDa. Thus, the present data shows that this protein is expressed in human corneal fibroblasts.

Some of the proteins were present in different isoforms. These proteins included actin (*e.g.* spots 14–17, 152, 153,

176, 186, and 198; Fig. 2*C*), α-enolase (*e.g.* spots 110, 131, 140, 146, 175, 200, 244, and 246; Fig. 2, *C* and *D*), glyceraldehyde 3-phosphate dehydrogenase (spots 222, 231, 238, 240, 241, and 242; Fig. 2*D*), 78-kDa glucose-regulated protein (BiP) (*e.g.* spots 12, 21, 46, and 89; Fig. 2*A*), phosphoglycerate kinase 1 (spots 108, 119, 122, 123, and 248; Fig. 2, *C* and *D*), protein disulfide isomerase (prolyl 4-hydroxylase β subunit) (*e.g.* spots 149, 151, 166, and 204; Fig. 2*C*), protein disulfide isomerase A3 (*e.g.* spots 18, 28, 32, 33, 50, and 79; Fig. 2*A*), pyruvate kinase M1 or M2 (*e.g.* spots 245, 247, 249, and 250; Fig. 2*D*), superoxide dismutase (Mn) (*e.g.* spots 115, 168, 213, and 233; Fig. 2*D*), triosephosphate isomerase (*e.g.* spots 25, 156, 211, and 228; Fig. 2*D*), and vimentin (*e.g.* spots 7, 8, 9–11, 147, 159, 162, and 164; Fig. 2*C*) (Table I).

Among the 118 identified proteins, five proteins have previously been classified as corneal enzyme-crystallins in corneal epithelial cells (Table II). Thus, nonfilamentous actin represents ~15% of the water-soluble protein of the zebrafish cornea (29, 46), peptidyl-prolyl *cis-trans* isomerase A represents 5–10% of the soluble protein in chicken, α-enolase is a prominent protein in mammals and chicken, glutathione *S*-transferase-like protein predominates in the squid cornea (26), while isocitrate dehydrogenase represents about 13% of the total bovine corneal epithelial soluble protein (28).

DISCUSSION

At present, the prevalent hypothesis of corneal cellular transparency and the development of cellular opacification during wound-healing involves enzyme-crystallins, which are highly expressed in corneal epithelium and keratocytes. A high level of enzyme-crystallins in corneal keratocytes are believed to contribute to the transparency and refractive properties of the cells by minimizing the refractive index fluctuations between the cytoplasm and the extracellular milieu (17, 47). Accordingly, corneal cellular haze development is thought to be related to low levels of water-soluble enzyme-crystallins in the cytoplasm of the reflective keratocyte phenotype. In the present study, 118 distinct proteins of the most abundant water-soluble proteins in human corneal fibroblasts were identified. Most of the identified proteins are housekeeping proteins common to most other cell types from nontransparent tissues. Thus, a significant number of the identified proteins are also expressed by other fibroblastic cells such as dermal fibroblasts (48, 49) and MRC5 fibroblasts (50) (visit proteomics.cancer.dk/jecelis/human_data_select.html). This finding may reflect a common mechanism of light scattering from reflective cells.

Corneal Enzyme-Crystallins and Various Isoforms—Densitometry of 1D gels revealed that no single band exceeds 5% of the total soluble protein fraction, which is the qualifying property of a corneal enzyme-crystallin according to the current definition. Because the definition of enzyme-crystallins is rather loose and does not consider the presence of various molecular mass isoforms (30), this result indicates that cul-
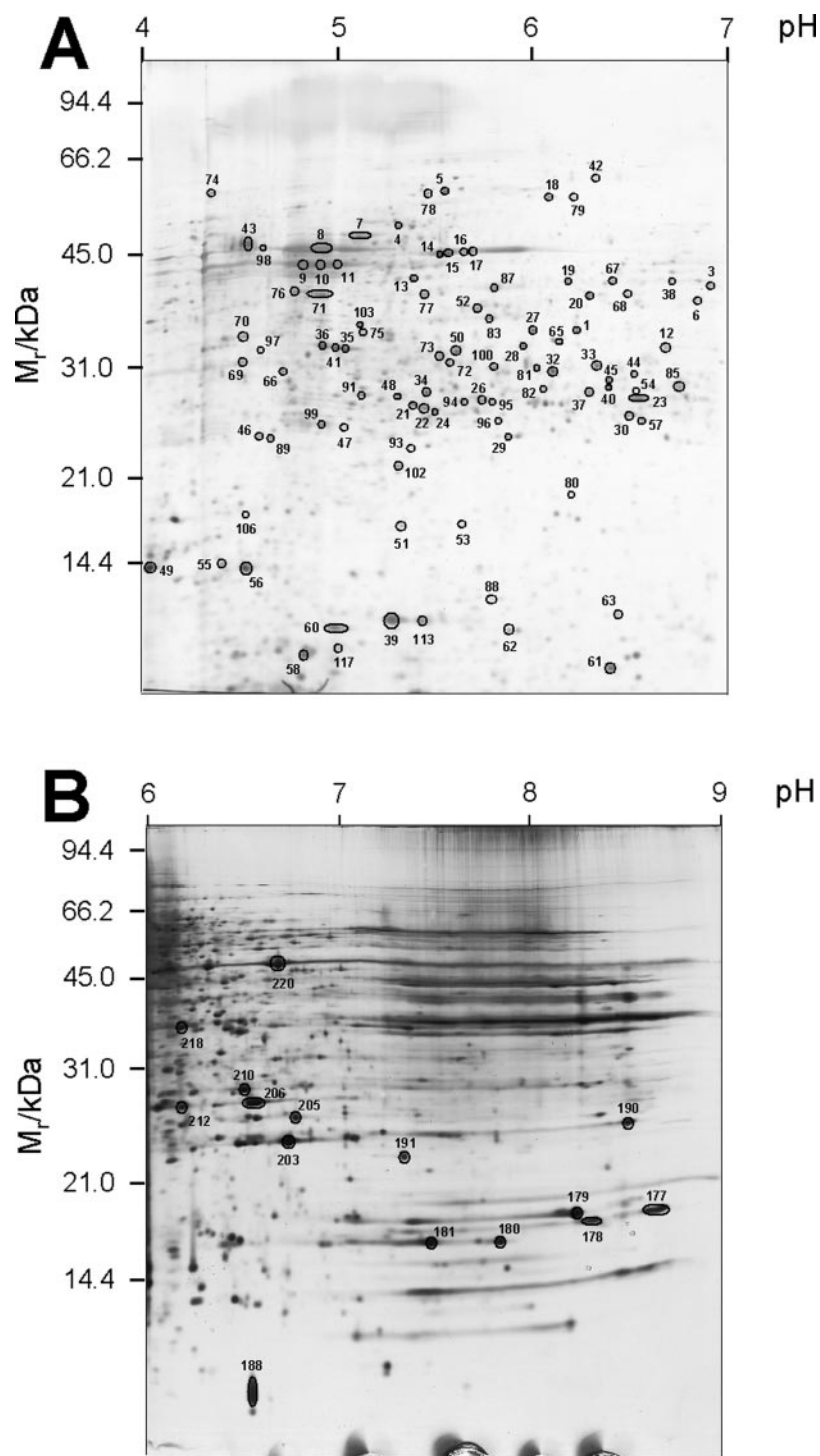
Fig. 2. **2D PAGE of the soluble fraction from human corneal fibroblasts.** 2D gels (18 × 23.4 cm) of the soluble proteome from human corneal fibroblasts using pH gradients (*A*) 4–7, (*B*) 6–9, (*C*) 4.5–5.5, and (*D*) 5.5–6.7. All 2D gels are silver-stained. The annotations in the gels refer to the spot ID numbers in Table I.

tured human corneal fibroblasts do not contain enzyme-crystallins. In addition, neither ALDH3A1 nor TKT were found among the most abundant water-soluble proteins, indicating that these enzyme-crystallins are not present or only expressed at low levels, which is in accordance with previous results (51).

The proteome analysis identified five proteins that have

previously been classified as enzyme-crystallins in the corneal epithelium of various species (Table II). In a previous study (26), the full-length α-enolase (~48 kDa) was shown to be highly expressed in human corneal epithelium. The finding of at least eight α-enolase isoforms (*e.g.* spots 110, 131, 140, 146, 175, 200, 244, and 246; Fig. 2, *C* and *D*) in human corneal fibroblasts indicates that this glycolytic enzyme/enzyme-crys-
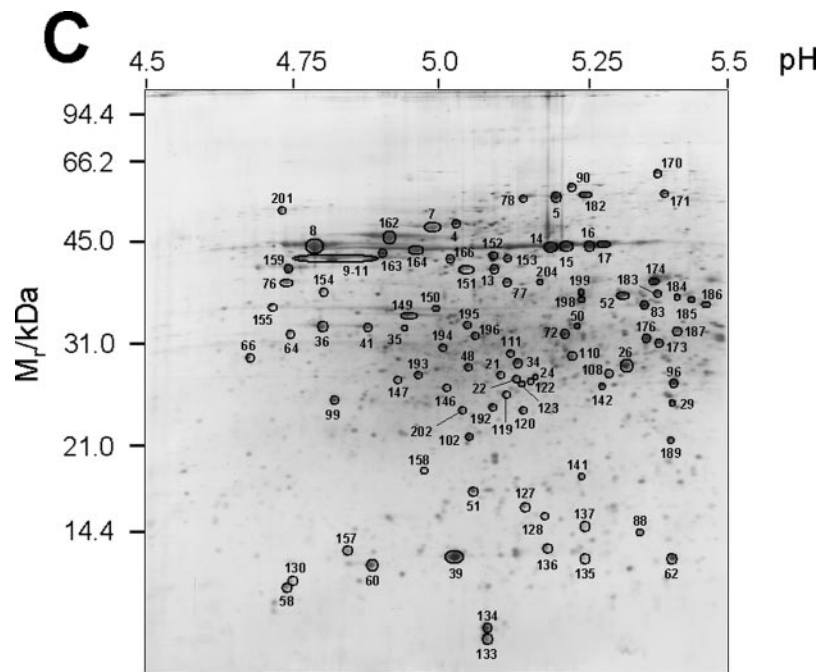
FIG. 2— *continued*
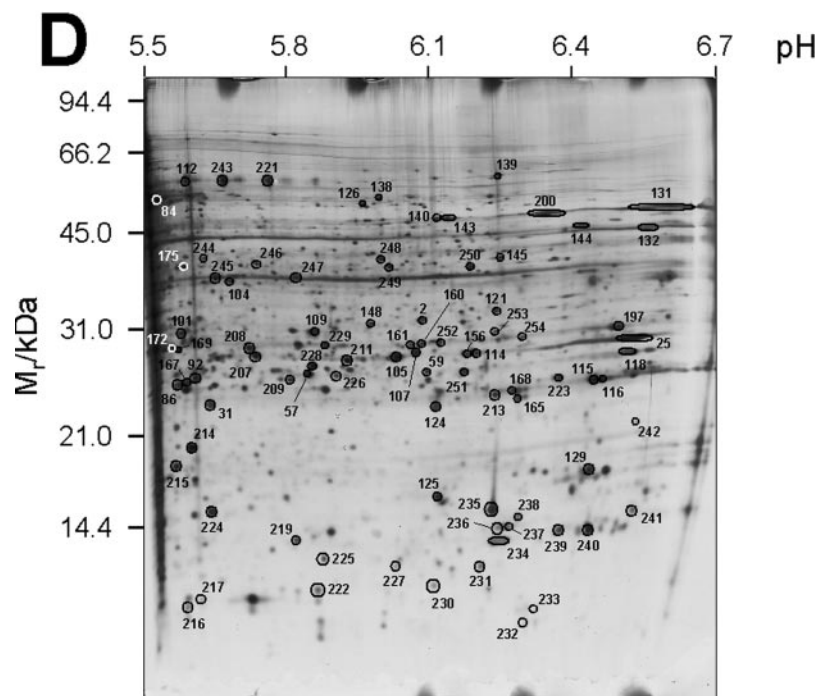
tallin is rather abundant also in corneal fibroblasts, but it remains unknown why it is present in several different isoforms. However, the 37-kDa isoforms can be explained by the finding that an alternative translation of the full-length α-enolase mRNA can produce a 37-kDa isoform, which is known to bind the c-*myc* promoter and function as a transcriptional repressor (52). In addition, the isoforms with similar molecular masses but different pI values may be explained by post-translational modifications such as phosphorylation. Thus, the isoforms of α-enolase (spots 175/246, and 140/200/131; Fig. 2*D*), peptidyl-prolyl *cis-trans* isomerase A (spots 181 and 180; Fig. 2*B*), actin (*e.g.* spots 14–17, and 152/153; Fig. 2*C*), and the isoforms of triosephosphate isomerase (*e.g.* spots 114, 211, and 228; Fig. 2*D*) may reflect post-translational modifications.

TABLE I

Proteins identified in the soluble fraction from human corneal fibroblasts

Acc. no., accession number in the Swiss-Prot/TrEMBL or NCBInr databases. FL_{aa}, number of residues in the full-length (precursor) protein according to the protein databases. M_{th}, theoretical molecular mass (kDa) of the full-length protein. M_{ob}, observed molecular mass (kDa). pI_{th}, theoretical pI of the full-length protein. pI_{ob}, observed pI. M_{ob} and pI_{ob} are determined from gels *C* and *D* in Fig. 2 when possible. Function (capital letters), proteins are categorized according to function as reported in the current literature. C, cytoskeleton-associated proteins and cell motility; B, proteinase inhibition; D, DNA replication and repair; F, protein folding and degradation; I, cell immune defense, antigen presentation, and endocytosis; L, signal transduction; M, metabolism; O, redox regulation and oxidative stress defense; P, cell proliferation, differentiation, and apoptosis; S, secretory pathway, transport from ER and Golgi, and exocytosis; T, other functions including transcription, splicing, ion transport, osmotic regulation, etc; U, unknown; Y, protein synthesis. Localization (small letters), cellular localization as reported in the current literature. a, associated with plasma membrane; c, cytosol; e, ER; l, lysosome; m, mitochondrion; n, nuclear; p, peroxisome; r, sarcoplasmic reticulum; s, secreted. Gel and spot IDs correspond to those given in the annotated gel images in Fig. 2. Covered fragment, fragment covered by the matching peptides in peptide fingerprinting or by MS/MS (underlined).

Protein	Acc. no.	Function and localization	$FL_{aa}/M_{th}/pI_{th}$	M_{ob}/pI_{ob}	Gel ID	Spot ID	Covered fragment
Actin, β or γ	P02570 or P02571	C/c	375/41.7/5.3	44.6/5.2	A/C	14	A19-K373
				44.6/5.2	A/C	15	A29-K373
				44.6/5.3	A/C	16	A19-K373
				44.6/5.3	A/C	17	A29-K373
				35.5/5.4	A/C	83	V96-R372
				42.6/5.1	C	152	A19-K336
				42.5/5.1	C	153	A19-K336
				31.5/5.4	C	176	G63-K373
				35.5/5.5	C	186	V96-R372
				36.0/5.2	C	198	I85-K336
				37.0/5.2	C	199	I85-K336
Acyl-CoA-binding protein	P07108	M/c/n	87/9.9/6.1	9.5/5.6	D	216	S2-K67
Alcohol dehydrogenase [NADP$^+$] (Aldo-keto reductase 1A1)	P14550	M/c	325/36.8/6.3	40.9/6.2	D	145	M14-K308
α-Actinin 1	P12814	C/c	892/103.5/5.2	29.1/4.7	A/C	66	I656-R863
Annexin A1	P04083	P/L/T/c/a/n	346/38.8/6.6	28.7/5.1	A/C	34	Q10-R228
				28.3/5.0	A/C	48	G30-R228
				37.2/6.2	B	218	Q10-R228
Annexin A2	P07355	P/L/T/c/a	339/38.7/7.6	17.5/5.6	A	53	L11-R168
				27.3/5.8	A	95	A29-R205
				33.3/6.2	D	121	L11-R245
				18.9/5.2	C	141	L11-R168
Annexin V	P08758	P/L/T/c/a	320/35.8/5.0	34.3/5.1	A	75	G7-R285
ATP synthase α chain, mitochondrial precursor	P25705	M/m	553/59.8/9.2	14.3/4.8	C	157	T46-K194
ATP synthase β chain, mitochondrial precursor	P06576	M/m	529/56.5/5.3	48.9/5.0	A/C	4	L95-K480
ATP synthase D chain, mitochondrial precursor	O75947	M/m	161/18.5/5.2	24.5/5.1	C	120	T10-K121
β_2-microglobulin, precursor	P01884	I/s	119/13.8/6.1	10.8/6.1	D	230	<u>V102-K111</u>
Calcyclin (S100A6)	P06703	P/F/L/r/n	90/10.2/5.3	9.1/5.1	C	133	<u>E41-R55</u>
				9.9/5.1	C	134	<u>E41-R55</u>
Calgizzarin (S100A14 or S100A11p)	NP_066369	U/u	102/11.4/7.8	8.9/6.4	A	61	I4-K78
Calmodulin	P02593	L/S/P/c	149/16.8/4.1	14.6/4.0	A	49	E15-K149
Calreticulin, precursor	P27797	F/S/e	417/48.3/4.3	56.8/4.3	A	74	E25-K286
Calumenin, precursor	O43852	S/e/s	315/37.1/4.5	47.0/4.5	A	43	V28-K284
Cathepsin B, precursor	P07858	I/P/F/l	339/38.8/5.9	27.6/5.1	A/C	22	I210-R331
				31.8/5.5	A	73	L80-R331
				26.9/5.7	A	94	I210-R331
Cathepsin D, precursor	P07339	P/L/F/I/l	412/45.0/6.1	31.9/5.2	A/C	72	Y123-R411
				31.0/5.9	D	109	Q185-R411
				32.3/5.4	C	187	Y123-R411
				33.2/5.1	C	196	Q185-R411
Cell division control protein 42 homolog (G25K GTP-binding protein)	P21181	C/P/L/c	191/21.7/5.8	23.6/5.6	D	31	<u>T108-R120</u>
				23.6/6.1	D	124	<u>T108-R120</u>
Chloride intracellular channel protein 1 (CLIC1)	O00299	O/T/n/c	241/27.3/5.1	32.8/5.0	C	195	I21-K238
Chloride intracellular channel protein 4 (CLIC4)	Q9Y696	C/P/c/m/n	253/29.0/5.5	31.1/5.4	C	173	A25-R227
Clathrin light chain B	P09497	M/I/c/a/l	229/25.3/4.6	31.0/4.5	A	69	L96-K204

TABLE I—*continued*

Protein	Acc. no.	Function and localization	$FL_{aa}/M_{th}/pI_{th}$	M_{ob}/pI_{ob}	Gel ID	Spot ID	Covered fragment
Cofilin, non-muscle isoform	P23528	C/c/n	166/18.7/8.2	13.8/5.4	A/C	62	K34-K92
				19.6/8.3	B	179	A35-R146
Destrin	P18282	C/c/n	165/19.0/8.1	18.8/8.3	B	178	C23-K151
Dihydrolipoamide succinyltransferase component of 2-oxoglutarate dehydrogenase complex, mitochondrial precursor (E2)	P36957	M/m	453/49.0/9.0	22.0/5.0	A/C	102	D313-R325
Dynein light chain 2A or 2B, cytoplasmic	Q9NP97 or Q8TF09	C/P/c	96/10.9/6.6–6.9	10.2/5.6	D	217	D59-R70
Electron transfer flavoprotein β subunit (ETF-β)	P38117	M/m	255/28.1/8.2	26.5/5.3	C	142	E60-R233
Elongation factor 1-β (EF-1β)	P24534	Y/c	225/24.8/4.5	32.2/4.6	A	97	S8-K22
Elongation factor 2 (EF-2)	P13639	Y/c	858/96.1/6.4	11.9/6.0	D	227	A786-R801
Endoplasmic reticulum protein 29, precursor (ERp29)	P30040	F/S/e/s	261/29.0/6.8	29.8/6.5	A	44	G37-K253
				29.3/5.9	D	229	G37-K253
Endoplasmin, precursor (GRP94)	P14625	F/S/e	803/92.7/4.8	24.0/6.3	D	165	L494-R503
				51.3/4.7	C	201	T44-R448
α-Enolase	P06733	M/T/c/n	434/47.5/7.0	34.3/6.2	A	1	A33-K343
				38.0/6.8	A	6	A121-R372
				40.5/6.2	A	19	A33-K326
				27.6/5.2	A/C	24	A121-K343
				34.3/6.0	A	27	A33-K343
				24.6/5.0	A	47	L163-K343
				33.0/6.1	A	65	L163-K343
				41.0/6.4	A	67	G16-K343
				29.5/5.2	C	110	F106-K343
				51.2/6.6	D	131	G16-R412
				47.9/6.1	D	140	G16-R412
				47.9/6.1	D	143	G16-R412
				26.5/5.0	C	146	L163-R327
				39.7/5.6	D	175	A33-R50
				49.5/6.3	D	200	G16-R412
				47.5/6.7	B	220	G16-R412
				40.9/5.6	D	244	G16-K326
				40.3/5.7	D	246	G16-K326
Enoyl-CoA hydratase, mitochondrial precursor	P30084	M/m	290/31.8/8.3	29.1/6.4	A	45	G42-R283
				29.3/5.7	D	208	G42-K273
Ferritin light chain	P02792	O/T/c/l	175/19.9/5.5	20.9/5.4	C	189	L155-R169
Galectin-1	P09382	P/C/s/n	135/14.9/5.3	13.8/5.0	A/C	39	D38-K130
				11.5/5.4	A	113	D38-R49
				13.6/5.2	C	135	V20-K130
				14.3/5.2	C	136	V20-R112
Glutathione S-transferase, mitochondrial precursor	Q9Y2Q3	O/m	226/25.5/8.5	14.3/6.3	D	237	H75-R225
Glutathione S-transferase P (GSTP1–1)	P09211	O/c	210/23.5/5.4	26.9/5.4	A/C	96	P2-K141
				25.4/5.6	D	167	F56-R71
Glutathione transferase ω 1 (GSTO 1–1)	P78417	O/c	241/27.8/6.2	31.0/5.6	D	101	S2-K220
				46.3/6.6	D	132	G12-R25
Glyceraldehyde 3-phosphate dehydrogenase	P04406	M/c	335/35.9/8.6	10.6/5.9	D	222	L310-R323
				11.9/6.2	D	231	L310-R323
				14.8/6.3	D	238	L67-R80
				14.1/6.4	D	240	L310-R323
				15.3/6.5	D	241	L310-R323
				22.0/6.5	D	242	L67-R80
Glyoxalase I (lactoylglutathione lyase)	Q04760	O/M/c	184/20.8/5.3	24.2/5.0	C	202	D29-K179
GTP-binding nuclear protein RAN (TC4)	P17080	P/T/c/n	216/24.6/7.0	27.2/6.8	B	205	Y39-R56
Heat shock cognate 71-kDa protein (Hsc71)	P11142	F/c	646/71.1/5.4	35.5/4.7	C	155	N540-K550
				43.3/4.9	C	163	T273-K550
				30.1/6.3	D	254	G4-K246
Heat shock protein 27-kDa	P04792	F/P/C/c	205/22.8/6.0	28.4/6.4	A	40	R5-R188
				15.7/5.2	C	137	L172-R188
				28.1/5.7	D	207	R5-R188

TABLE I—*continued*

Protein	Acc. no.	Function and localization	$FL_{aa}/M_{th}/pI_{th}$	M_{ob}/pI_{ob}	Gel ID	Spot ID	Covered fragment
Heterogeneous nuclear ribonucleoprotein H (hnRNP H)	P31943	T/n	449/49.5/5.9	26.5/5.9	D	226	H99-R114
				26.9/6.2	D	251	G17-R29
Heterogeneous nuclear ribonucleoprotein K (hnRNP K)	Q07244	T/c/n	463/51.2/5.4	35.2/5.1	A	103	T70-R86
Histidine triad nucleotide-binding protein 1	P49773	T/c/n	126/13.8/6.5	13.3/6.2	D	234	A8-R119
3-Hydroxyisobutyrate dehydrogenase, mitochondrial precursor	P31937	M/m	336/35.7/8.4	29.9/5.1	C	111	M150-R167
Hypothetical protein (fragment) (IL-25/SF20)	Q9BTK7	U/u	171/18.8/6.1	15.6/6.2	D	235	S99-K107
Isocitrate dehydrogenase [NADP⁺], cytoplasmic	O75874	M/O/c/p	414/46.9/6.5	47.1/6.4	D	144	I5-K400
78-kDa glucose-regulated protein, precursor (BiP)	P11021	F/S/e	654/72.4/5.1	32.6/6.7	A	12	V50-R214
				27.6/5.1	A/C	21	A298-K474
				24.0/4.6	A	46	G493-L654
				24.0/4.6	A	89	G493-L654
				16.4/5.2	C	128	K353-R367
				31.9/6.0	D	148	V50-K271
				30.3/5.0	C	194	V50-K271
60-kDa heat shock protein, mitochondrial precursor	P10809	F/m	573/61.2/5.7	54.9/5.2	A/C	5	A38-K516
				31.9/4.7	C	64	T206-R526
				54.0/5.1	A/C	78	D29-R526
				54.0/5.3	C	182	A38-R526
MIR-interacting saposin-like protein (MSAP)	NP_055070	C/P/c	182/21.0/4.8	19.5/5.0	C	158	S23-L182
Myosin alkali light chain isoform 1, smooth muscle and non-muscle	NP_066299	C/P/L/c	151/17.1/4.6	14.8/4.4	A	55	E14-K119
				14.6/4.5	A	56	E14-R146
Nuclear transport factor 2	P13662	T/c	127/14.6/5.1	10.1/5.0	A	117	N107-R120
Nucleophosmin (nucleolar phosphoprotein B23)	P06748	T/P/F/n	294/32.7/4.6	18.3/4.5	A	106	M81-R101
Nucleoside diphosphate kinase A	P15531	M/c/n	152/17.3/5.8	19.6/6.2	A	80	T7-R114
				17.1/5.1	C	127	F40-K128
				20.1/5.6	D	214	T7-K128
Nucleoside diphosphate kinase B	P22392	M/c/n	152/17.4/8.5	12.0/6.4	A	63	Q50-K143
				19.6/8.7	B	177	T7-K143
				13.6/5.8	D	219	Q50-K143
				14.1/6.4	D	239	D57-E152
Peptidyl-prolyl *cis-trans* isomerase (FKBP65)	Q96AY3	F/S/e	582/64.8/5.4	60.6/6.3	A	42	E58-R577
				57.1/5.6	D	112	A34-R577
				57.1/5.8	D	221	A34-R485
				57.1/5.7	D	243	A34-R577
Peptidyl-prolyl *cis-trans* isomerase A (cyclophilin A)	P05092	F/c	165/18.1/7.8	17.6/7.8	B	180	V2-E165
				17.6/7.5	B	181	V2-E165
Peroxiredoxin 1	Q06830	O/c	199/22.3/8.3	26.8/8.5	B	190	Q141-R151
Peroxiredoxin 2	P32119	O/c	198/22.1/5.4	24.8/5.4	A/C	29	I8-R150
Peroxiredoxin 3, mitochondrial precursor	P30048	O/m	256/28.0/7.7	25.6/6.5	A	30	T38-R214
				26.1/5.6	D	92	D171-R184
Peroxiredoxin 4	Q13162	O/c	271/30.8/5.9	28.4/6.1	A	82	T46-R223
Peroxiredoxin 5, mitochondrial precursor	P30044	O/m/p/c	214/22.3/8.9	16.4/6.1	D	125	E160-R176
Peroxiredoxin 6	P30041	O/c/l/s	224/25.0/6.0	28.4/6.8	A	85	F25-R174
				28.1/6.0	D	105	P2-K199
Phosphatidylethanolamine-binding protein	P30086	L/B/c/s	187/21.0/7.4	23.9/7.4	B	191	L63-R76
6-Phosphogluconolactonase (lactonase)	O95336	M/c	258/27.8/5.7	28.9/5.6	D	169	F41-R246
				28.9/5.6	D	172	E57-R72
Phosphoglycerate kinase 1	P00558	M/c	418/44.7/7.5	27.6/5.3	C	108	A200-K382
				25.9/5.1	C	119	I280-K297
				27.2/5.2	C	122	A107-K406
				26.9/5.2	C	123	V19-K406
				40.9/6.0	D	248	A107-R123
Phosphoglycerate mutase 1, isozyme B	P18669	M/c	254/28.8/6.8	31.5/6.5	D	197	H11-R240
				30.1/6.5	B	210	H11-R240
Phosphomannomutase 2	O15305	S/c	246/28.4/6.4	29.3/6.1	D	161	A2-S246

TABLE I—*continued*

Protein	Acc. no.	Function and localization	$FL_{aa}/M_{th}/pI_{th}$	M_{ob}/pI_{ob}	Gel ID	Spot ID	Covered fragment
Polymerase I and transcript release factor	NP_036364	T/n	390/43.5/5.5	23.1/5.4	A	93	I61-R78
				24.5/5.1	C	192	K137-R147
Prefoldin subunit 1	O60925	F/c	122/14.2/6.3	12.4/5.9	D	225	L29-R39
Profilin I	P07737	C/c	140/15.1/8.4	11.9/4.8	A/C	58	D27-K105
				12.3/4.8	C	130	D27-K105
Prohibitin	P35232	P/c	272/29.8/5.6	30.6/5.8	A	100	A220-R239
				31.1/5.4	C	173	F12-R253
Prolyl 4-hydroxylase α-1 subunit precursor	P13674	F/S/e	534/61.3/5.7	29.4/6.1	D	160	D105-E534
				29.7/6.1	D	252	S383-R396
Prolyl 4-hydroxylase β subunit (Protein disulfide isomerase), precursor	P07237	F/e	508/57.4/4.8	40.8/5.1	A/C	13	K31-R345
				38.6/5.1	A/C	77	L70-K370
				34.1/5.0	C	149	L79-R345
				40.8/5.0	C	151	L70-R345
				42.0/5.0	C	166	L79-K370
				38.6/5.2	C	204	V82-K386
Protease inhibitor 6	P35237	B/c	376/42.9/5.2	37.5/4.8	C	154	S62-K299
Proteasome activator 28-α	Q06323	F/I/c	249/28.9/5.8	30.2/6.0	A	81	I110-R213
Proteasome activator 28-γ	Q12920	F/I/c	254/29.6/5.7	26.1/5.8	D	209	L13-K237
Proteasome subunit α type 1	P25786	F/c/n	263/29.8/6.2	32.4/6.1	D	2	N4-R242
Proteasome subunit α type 2	P25787	F/c/n	234/25.9/7.1	28.9/6.5	D	118	G5-R219
Proteasome subunit α type 6	P34062	F/c/n	246/27.8/6.3	28.5/6.1	D	107	H12-K164
Proteasome subunit β type 2	P49721	F/c/n	201/23.0/6.5	26.1/6.4	D	223	V20-R181
Proteasome subunit β type 3	P49720	F/c/n	205/23.2/6.1	26.5/5.8	A/D	57	N18-K192
Protein disulfide isomerase A3, precursor (ERp57)	P30101	F/S/e/c/n	505/57.1/6.0	55.9/6.1	A	18	Q131-R482
				32.6/5.9	A	28	R62-K271
				30.2/6.1	A	32	K305-R482
				30.6/6.3	A	33	F215-R482
				32.8/5.2	A/C	50	R62-R280
				55.9/6.2	A	79	R62-R448
				52.1/5.5	D	84	R62-K496
				31.0/6.2	D	253	A174-K496
Protein-L-isoaspartate (D-aspartate) O-methyltransferase	P22061	F/O/c	227/24.7/6.8	26.5/6.1	D	59	A82-R98
Pyruvate dehydrogenase E1 component β subunit, mitochondrial precursor	P11177	M/m	359/39.5/6.2	37.0/5.4	C	183	E259-R269
Pyruvate kinase, M1 or M2 isozyme	P14618 or P14786	M/c	531/57.9/8.0	40.0/6.9	A	3	L33-R294
				38.4/6.3	A	20	L33-R376
				28.0/6.3	A	37	L33-R246
				40.5/6.7	A	38	L33-K305
				38.9/6.5	A	68	L33-R294
				38.0/5.7	D	245	L33-K336
				38.0/5.8	D	247	L33-K336
				39.7/6.0	D	249	R279-R294
				39.7/6.2	D	250	L33-K497
Retinoic acid-binding protein II, cellular (CRABP-II)	P29373	L/P/c	138/15.7/5.4	15.2/5.3	A/C	88	V68-K83
Rho GDP-dissociation inhibitor 1	P52565	L/P/c	204/23.3/5.0	27.6/5.0	C	193	S34-K199
60S acidic ribosomal protein P0	P05388	Y/c	317/34.4/5.7	37.4/5.7	D	104	I17-K297
snRNP core protein D3	P43331	T/c/n	126/13.9/10.3	8.7/6.3	D	232	V55-R64
40S ribosomal protein S12	P25398	Y/c	132/14.7/6.4	14.3/6.2	D	236	T24-R33
40S ribosomal protein Sa (LBP/p40)	P08865	Y/P/c/n	295/33.0/4.8	33.8/4.5	A	70	F90-R180
Stress-induced phosphoprotein 1 (Hop or Sti1)	P31948	F/P/c/p	543/63.2/6.4	58.2/6.2	D	139	A14-R543
Stress-70 protein, mitochondrial precursor (mortalin)	P38646	P/F/L/m/c/a/e	679/74.0/6.0	58.0/5.2	C	90	A147-K595
				35.1/5.0	C	150	S469-K485
				62.6/5.4	C	170	G53-K563
Succinyl-CoA:3-ketoacid-coenzyme A transferase, mitochondrial precursor	P55809	M/m	520/56.6/7.1	53.0/6.0	D	138	G84-R104

TABLE I—*continued*

Protein	Acc. no.	Function and localization	$FL_{aa}/M_{th}/pI_{th}$	M_{ob}/pI_{ob}	Gel ID	Spot ID	Covered fragment
Superoxide dismutase (Cu-Zn)	P00441	O/c	154/16.0/5.7	18.6/5.6	D	215	G11-K24
Superoxide dismutase (Mn), mitochondrial precursor	P04179	O/m	222/24.9/8.4	25.8/6.4	D	115	G76-R216
				25.8/6.5	D	116	A203-R216
				25.0/6.3	D	168	A203-R216
				25.2/6.7	B	203	H54-R216
				24.3/6.2	D	213	H54-R216
				9.3/6.3	D	233	G76-K89
T-complex protein 1, β subunit (TCP-1-β)	P78371	F/c	535/57.5/6.0	18.1/5.1	A/C	51	L26-K170
				51.2/6.0	D	126	L26-R516
T-complex protein 1, ϵ subunit (TCP-1-ϵ)	P48643	F/c	541/60.1/5.4	55.9/5.4	D	171	I133-R525
Thioredoxin	P10599	O/c	105/12.0/4.8	13.4/4.9	A/C	60	T9-V105
Transforming protein RhoA (H12)	P06749	L/c/a	193/22.1/5.8	25.4/5.6	D	86	L8-R176
Transgelin	Q01995	C/P/c	201/22.5/8.9	18.3/6.4	D	129	L30-K121
Transitional endoplasmic reticulum ATPase (TER ATPase)	P55072	S/T/c/n	806/90.0/5.1	36.0/5.4	C	185	M46-R53
Translationally controlled tumor protein (TCTP)	P13693	P/Y/c	172/19.7/4.8	25.2/4.8	A/C	99	I20-K34
Triosephosphate isomerase	P00938	M/c	249/26.8/6.5	27.3/6.5	A	23	K19-K188
				30.1/6.5	D	25	K6-R206
				28.0/6.5	A	54	V34-K219
				28.5/6.2	D	114	V34-R206
				28.5/6.2	D	156	K6-K219
				28.6/6.5	B	206	K19-K219
				27.7/5.9	D	211	V34-K219
				28.2/6.2	B	212	K6-R206
				27.3/5.9	D	228	K19-K219
Tropomyosin α-3 chain	P06753	C/c	247/29.1/4.7	32.7/4.9	A/C	35	K13-D247
				32.8/4.9	A/C	41	K13-D247
Tropomyosin α-4 chain	P07226	C/c	248/28.6/4.7	32.8/4.8	A/C	36	K13-I248
Tropomyosin β chain	P07951	C/c	284/33.0/4.7	38.9/4.9	A	71	K77-L284
				38.6/4.7	A/C	76	L13-R178
Tubulin α-1 chain	P05209	C/c	451/50.8/4.9	40.0/5.8	A	87	T41-K280
Tubulin α-6 chain	Q9BQE3	C/c	449/49.9/5.0	38.6/5.4	C	174	T41-K280
Tubulin β-4 chain	Q13509	C/c	450/50.9/4.8	36.5/5.4	C	184	I47-K58
Tubulin β-5 chain	P05218	C/c	444/50.1/4.8	37.0/5.3	A/C	52	F20-K297
Ubiquitin	P02248	F/c/n	76/8.6/6.6	9.3/6.5	B	188	E64-R72
Ubiquitin-conjugating enzyme E2 N (Ubc13)	Q16781	D/F/c/n	152/17.2/6.1	15.3/5.6	D	224	L15-R141
Ubiquitin C-terminal hydrolase-L1	P09936	F/c	223/25.2/5.3	28.3/5.3	A/C	26	M1-K195
Vimentin	P08670	C/c	466/53.8/5.0	48.1/5.0	A/C	7	L79-K439
				44.5/4.8	A/C	8	T101-R424
				43.3/4.7	A/C	9	L79-R378
				43.3/4.8	A/C	10	L79-R378
				43.3/4.9	A/C	11	T101-R424
				27.6/5.1	A	91	D271-E466
				45.7/4.6	A	98	T101-R424
				27.2/4.9	C	147	F114-R440
				40.8/4.7	C	159	L79-K402
				45.9/4.9	C	162	L79-R440
				43.9/5.0	C	164	L79-R424

Metabolism—The transition of the quiescent keratocyte into the corneal fibroblast phenotype is characterized by development of extensive rough endoplasmic reticulum (ER), a prominent Golgi apparatus, and an increase in the number of vesicles and mitochondria (13, 45) reflecting an increase in the requirement of protein trafficking and respiration. This was confirmed by the identification of several mitochondrial metabolic enzymes in the soluble fraction from the corneal fibroblast. These proteins are involved in oxidative decarboxylation of pyruvate (E1 component β subunit of the pyruvate dehydrogenase complex), fatty acid oxidation (enoyl-CoA hydratase), the citric acid cycle (E2 component of the mitochondrial 2-oxoglutarate dehydrogenase complex), the respiratory chain (β subunit of electron transfer flavoprotein), and the ADP

TABLE II

Proteins in human corneal fibroblasts classified as enzyme-crystallins in corneal epithelium

Enzyme-crystallin	Species	Ref.
Actin, non-filamentous (in complex with gelsolin)	Zebrafish	29
α-Enolase	Human, mouse, chicken	26
Isocitrate dehydrogenase	Bovine	28
Glutathione *S*-transferase	Squid	26
Peptidyl prolyl *cis-trans* isomerase A	Chicken	26

phosphorylation (ATP synthase chains). In addition, succinyl-CoA-3-ketoacid-coenzyme A transferase, which is a key enzyme for ketone body catabolism, was found.

Also several enzymes from the glycolytic pathway were identified. Thus, in addition to α-enolase, these included triosephosphate isomerase, glyceraldehyde 3-phosphate dehydrogenase, phosphoglycerate kinase 1, phosphoglycerate mutase 1B, and pyruvate kinase. In addition, 6-phosphogluconolactonase from the oxidative branch of the pentose phosphate pathway was found. Other metabolic enzymes included nucleoside diphosphate kinases, isocitrate dehydrogenase, and an alcohol dehydrogenase, isozyme 1A1. Thus, the present protein identifications are in accordance with a high metabolic activity in corneal fibroblasts. Interestingly, all six isoforms of glyceraldehyde 3-phosphate dehydrogenase had molecular masses and pI values (M_{ob} ~10–22 kDa, pI$_{ob}$ ~5.9–6.5) much smaller than the theoretical values (M_{th} ~36 kDa, pI$_{th}$ ~8.6), which indicate profound fragmentation of this enzyme (Table I; Fig. 2D).

The Secretory Pathway—The secretory pathway involves ER luminal proteins (Table I) assisting the folding and processing of secreted proteins. In the present study, protein disulfide isomerases, peptidyl-prolyl *cis-trans* isomerases, and molecular chaperones within the ER lumen were found. Protein disulfide isomerase A3 stimulates the formation and rearrangement of disulfide bonds in proteins, while peptidyl-prolyl *cis-trans* isomerase (FKBP65) catalyzes the *cis-trans* isomerization of the peptidyl-prolyl residue and facilitates the folding of secretory proteins during protein synthesis. In addition, the ER molecular chaperones, endoplasmin, ER protein 29, and 78-kDa glucose-regulated protein (BiP) are known to prevent aggregation of the secretory proteins.

Proteins involved in modification of secretory proteins are also present in the soluble fraction from corneal fibroblasts. Prolyl 4-hydroxylase (α-1 and β subunits) catalyzes the post-translational hydroxylation of proline in collagen and other proteins, and the β subunit is also a protein disulfide isomerase. Some secretory proteins are γ-carboxylated in the ER lumen by a system converting glutamate into γ-carboxyglutamate. The function of calumenin is not clear, but it has been shown to inhibit the vitamin-K-dependent γ-carboxylation of proteins in the ER lumen (53). Phosphomannomutase 2 is a cytosolic enzymes converting mannose 6-phosphate (man-6-P) to mannose-1-phosphate (man-1-P), which is required for the initial steps of protein glycosylation performed in the ER lumen and Golgi apparatus.

The finding of key enzymes involved in protein folding, proline hydroxylation, and glycosylation of secretory proteins is in accordance with the wound-healing process accomplished by corneal fibroblasts.

Identification of Hypothetical Protein/IL-25—The hypothetical human protein (accession number Q9BTK7, TrEMBL entry) revealed high homology to the novel mouse IL-25/SF20, which is a bone marrow stroma-derived growth factor. According to the previous findings, IL-25/SF20 is a secretory protein that stimulates cell proliferation (54, 55). Interestingly, recent reports have shown that both the corneal epithelium and stroma contain a significant number of resident bone marrow-derived cells such as macrophages and dendritic cells (56, 57). The bone marrow-derived cells are highly efficient in antigen presentation and initiate immune responses that are critical in corneal inflammation and allograft rejection. The identified human homologue of the mouse bone marrow stroma-derived growth factor IL-25/SF20 in corneal fibroblasts may play a regulatory role in the wound-healing process, which could include activation and transition of the resident bone marrow-derived cells in the corneal stroma.

Oxidative Stress Defense—Reactive oxygen species (ROS) are cytotoxic because they react with lipids and carbohydrates to generate highly reactive agents, damage DNA, and irreversible oxidize proteins that can lead to protein-protein cross-linking, fragmentation, unfolding and degradation, or formation of protein aggregates (58, 59). UV radiation is an exogenous source of ROS, while metabolic enzyme systems such as the respiratory chain are important endogenous sources of ROS and reactive cytotoxic agents (60). Thus, the many mitochondria in proliferating corneal fibroblasts compared with quiescent keratocytes presumably result in a higher level of oxidative stress in fibroblasts than in keratocytes. In accordance, several mitochondrial and cytosolic proteins involved in the redox regulation and protection against oxidative stress were identified in corneal fibroblasts. These proteins included mitochondrial and cytoplasmic glutathione *S*-transferases, thioredoxin, and several cytoplasmic and mitochondrial peroxiredoxins that play important roles in eliminating various peroxides formed during metabolism. In addition, mitochondrial superoxide dismutase (Mn) and superoxide dismutase (Cu-Zn) catalyzing the conversion of O_2^- radicals into hydrogen peroxide were found. Glyoxalase I is part of the glyoxalase system, which catalyzes the conversion of reactive aldehydes into acids and thereby detoxifies the cytosol. The fact that several of the identified proteins are involved in defense against oxidative stress indicates that the corneal fibroblasts senses oxidative stress, and it is reasonable to believe that the level of ROS generated endogenous is higher in proliferating corneal fibroblasts than in quiescent keratocytes.

Protein Folding and Degradation—Molecular chaperones and the protein degradation machinery are cellular protection systems that assist protein folding and prevent the accumulation of unfolded and damaged proteins. In the present study, both cytosolic and mitochondrial proteins involved in proteins folding and degradation were identified.

Prefoldin is a cytosolic chaperone that delivers unfolded protein, principally actins and tubulins, to the cytosolic chaperonin T-complex protein 1, which is essential for the folding of these cytoskeleton proteins (61). Hsp27 is an ubiquitously expressed member of the small heat shock proteins and has been implicated in various functions including cellular resistance during heat shock, oxidative stress, cytokine treatment, and is involved in cytoskeleton organization. Stress-induced phosphoprotein 1 is similar to the cytoplasmic yeast heat shock protein STI1 that is known to interact with hsp90 and hsp70 and regulate their ATPase activities. In addition, the cytosolic heat shock cognate 71-kDa protein was found. Mitochondrial 60-kDa heat shock protein is implicated in mitochondrial protein import and prevents unfolding under mitochondrial stress conditions, while mitochondrial stress-70 protein may be a chaperone.

The ubiquitin (Ub)-proteasome system catalyzes the destruction of unfolded or impaired proteins generated in cells. It has previously been shown that the Ub-proteasome system is induced during the phenotypic transition from keratocyte to fibroblast and that the higher levels of free Ub, Ub-protein conjugates, and the 26S proteasome in corneal fibroblasts were maintained during subculturing (51). Thus, the corneal fibroblast has a persisting pool of Ub conjugates targeted to the 26S proteasome for degradation. These results are consistent with the present findings of several proteins from the Ub-proteasome system including proteasome subunits, free Ub, Ub-conjugating enzyme, and Ub C-terminal hydrolase. The abundance of free Ub and proteasome subunits in subcultured corneal fibroblasts could indicate that the Ub-proteasome system in corneal fibroblasts is required for degradation of damaged or unfolded proteins rather than for protein degradations associated with cell transformation and differentiation as suggested for TKT (51). Thus, the present results in combination with the previous findings might indicate that the requirement of protein degradation, which could include the degradation of oxidized proteins, is higher in corneal fibroblasts than in keratocytes. However, certain oxidized proteins and severe oxidized proteins are poor substrates of the proteasome, which can lead to accumulation of oxidized protein aggregates in intracytoplasmic inclusions as observed in some diseases (62, 63).

Perspectives—Increased knowledge on the various keratocyte phenotypes is important for understanding corneal physiology and pathophysiology. The biochemical mechanisms regulating cellular transparency of the cornea are not fully understood. This study has applied a proteomic approach to identify soluble cellular components in primary corneal fibroblasts that are responsible for the cellular haze observed following corneal injury. Most of the identified proteins are common to other nontransparent fibroblastic cells from other tissues. The rather prominent finding of multiple proteins involved in oxidative stress defense, protein folding, and degradation in corneal fibroblasts provides the basis to propose that protein unfolding induced by oxidative stress may participate in the backscattering of light from this keratocyte phenotype. In that respect, it should be noted that oxidative stress is know to cause cataract owing to oxidation of lens proteins and formation of light-scattering, high-molecular-mass protein aggregates (64). Thus, it is possible that development of corneal cellular haze during wound-healing could somehow be reminiscent to the development of oxidative stress-induced opacity in the crystalline lens. Further studies are needed to explore this hypothesis.

‖ To whom correspondence should be addressed: Department of Ophthalmology, Aarhus University Hospital, Nørrebrogade 44, 8000 Aarhus C, Denmark. Tel.: 45-89493227; Fax: 45-86121653; E-mail: tmp@akhphd.au.dk.

REFERENCES

1. Marshall, G. E., Konstas, A. G., and Lee, W. R. (1991) Immunogold fine structural localization of extracellular matrix components in aged human cornea. II. Collagen types V and VI. *Graefes Arch. Clin. Exp. Ophthalmol.* **229,** 164–171
2. Birk, D. E., Fitch, J. M., Babiarz, J. P., Doane, K. J., and Linsenmayer, T. F. (1990) Collagen fibrillogenesis in vitro: interaction of types I and V collagen regulates fibril diameter. *J. Cell Sci.* **95,** 649–657
3. Maurice, D. (1957) The structure and transparency of the cornea. *J. Physiol.* **136,** 263–286
4. Komai, Y., and Ushiki, T. (1991) The three-dimensional organization of collagen fibrils in the human cornea and sclera. *Invest. Ophthalmol. Vis. Sci.* **32,** 2244–2258
5. Gallagher, B., and Maurice, D. (1977) Striations of light scattering in the corneal stroma. *J. Ultrastruct. Res.* **61,** 100–114
6. Møller-Pedersen, T. (2004) Keratocyte reflectivity and corneal haze. *Exp. Eye Res.* **78,** 553–560
7. Møller-Pedersen, T., Cavanagh, H. D., Petroll, W. M., and Jester, J. V. (1998) Corneal haze development after PRK is regulated by volume of stromal tissue removal. *Cornea* **17,** 627–639
8. Møller-Pedersen, T., Li, H. F., Petroll, W. M., Cavanagh, H. D., and Jester,

J. V. (1998) Confocal microscopic characterization of wound repair after photorefractive keratectomy. *Invest. Ophthalmol. Vis. Sci.* **39,** 487–501

9. Cintron, C., Schneider, H., and Kublin, C. (1973) Corneal scar formation. *Exp. Eye Res.* **17,** 251–259

10. Cintron, C., and Kublin, C. L. (1977) Regeneration of corneal tissue. *Dev. Biol.* **61,** 346–357

11. Ross, R., Everett, N. B., and Tyler, R. (1970) Wound healing and collagen formation. *J. Cell Biol.* **44,** 645–654

12. Cionni, R. J., Katakami, C., Lavrich, J. B., and Kao, W. W. (1986) Collagen metabolism following corneal laceration in rabbits. *Curr. Eye Res.* **5,** 549–558

13. Jester, J. V., Rodrigues, M. M., and Herman, I. M. (1987) Characterization of avascular corneal wound healing fibroblasts. New insights into the myofibroblast. *Am. J. Pathol.* **127,** 140–148

14. Jester, J. V., Petroll, W. M., Barry, P. A., and Cavanagh, H. D. (1995) Expression of alpha-smooth muscle (α-SM) actin during corneal stromal wound healing. *Invest. Ophthalmol. Vis. Sci.* **36,** 809–819

15. Welch, M. P., Odland, G. F., and Clark, R. A. (1990) Temporal relationships of F-actin bundle formation, collagen and fibronectin matrix assembly, and fibronectin receptor expression to wound contraction. *J. Cell Biol.* **110,** 133–145

16. Møller-Pedersen, T., Cavanagh, H. D., Petroll, W. M., and Jester, J. V. (1998) Neutralizing antibody to TGFβ modulates stromal fibrosis but not regression of photoablative effect following PRK. *Curr. Eye Res.* **17,** 736–747

17. Jester, J. V., Møller-Pedersen, T., Huang, J., Sax, C. M., Kays, W. T., Cavanagh, H. D., Petroll, W. M., and Piatigorsky, J. (1999) The cellular basis of corneal transparency: Evidence for 'corneal crystallins'. *J. Cell Sci.* **112,** 613–622

18. Horwitz, J. (1992) Alpha-crystallin can function as a molecular chaperone. *Proc. Natl. Acad. Sci. U. S. A.* **89,** 10449–10453

19. Horwitz, J. (2003) Alpha-crystallin. *Exp. Eye Res.* **76,** 145–153

20. Wistow, G. (1993) Lens crystallins: Gene recruitment and evolutionary dynamism. *Trends Biochem. Sci* **18,** 301–306

21. Graw, J. (1997) The crystallins: Genes, proteins and diseases. *Biol. Chem.* **378,** 1331–1348

22. Delaye, M., and Tardieu, A. (1983) Short-range order of crystallin proteins accounts for eye lens transparency. *Nature* **302,** 415–417

23. Abedinia, M., Pain, T., Algar, E. M., and Holmes, R. S. (1990) Bovine corneal aldehyde dehydrogenase: The major soluble corneal protein with a possible dual protective role for the eye. *Exp. Eye Res.* **51,** 419–426

24. Verhagen, C., Hoekzema, R., Verjans, G. M., and Kijlstra, A. (1991) Identification of bovine corneal protein 54 (BCP 54) as an aldehyde dehydrogenase. *Exp. Eye Res.* **53,** 283–284

25. Cooper, D. L., Baptist, E. W., Enghild, J. J., Isola, N. R., and Klintworth, G. K. (1991) Bovine corneal protein 54K (BCP54) is a homologue of the tumor-associated (class 3) rat aldehyde dehydrogenase (RATALD). *Gene* **98,** 201–207

26. Cuthbertson, R. A., Tomarev, S. I., and Piatigorsky, J. (1992) Taxon-specific recruitment of enzymes as major soluble proteins in the corneal epithelium of three mammals, chicken, and squid. *Proc. Natl. Acad. Sci. U. S. A.* **89,** 4004–4008

27. Sax, C. M., Salamon, C., Kays, W. T., Guo, J., Yu, F. X., Cuthbertson, R. A., and Piatigorsky, J. (1996) Transketolase is a major protein in the mouse cornea. *J. Biol. Chem.* **271,** 33568–33574

28. Sun, L., Sun, T. T., and Lavker, R. M. (1999) Identification of a cytosolic NADP⁺-dependent isocitrate dehydrogenase that is preferentially expressed in bovine corneal epithelium. A corneal epithelial crystallin. *J. Biol. Chem.* **274,** 17334–17341

29. Xu, Y. S., Kantorow, M., Davis, J., and Piatigorsky, J. (2000) Evidence for gelsolin as a corneal crystallin in zebrafish. *J. Biol. Chem.* **275,** 24645–24652

30. Piatigorsky, J. (1998) Gene sharing in lens and cornea: facts and implications. *Prog. Retin. Eye Res.* **17,** 145–174

31. Nees, D. W., Wawrousek, E. F., Robison, W. G., Jr., and Piatigorsky, J. (2002) Structurally normal corneas in aldehyde dehydrogenase 3a1-deficient mice. *Mol. Cell. Biol.* **22,** 849–855

32. Xu, Z. P., Wawrousek, E. F., and Piatigorsky, J. (2002) Transketolase haploinsufficiency reduces adipose tissue and female fertility in mice. *Mol. Cell. Biol.* **22,** 6142–6147

33. Lee, S. M., Koh, H. J., Park, D. C., Song, B. J., Huh, T. L., and Park, J. W. (2002) Cytosolic NADP⁺-dependent isocitrate dehydrogenase status modulates oxidative damage to cells. *Free Radic. Biol. Med.* **32,** 1185–1196

34. Pappa, A., Chen, C., Koutalos, Y., Townsend, A. J., and Vasiliou, V. (2003) Aldh3a1 protects human corneal epithelial cells from ultraviolet- and 4-hydroxy-2-nonenal-induced oxidative damage. *Free Radic. Biol. Med.* **34,** 1178–1189

35. Pappa, A., Estey, T., Manzer, R., Brown, D., and Vasiliou, V. (2003) Human aldehyde dehydrogenase 3A1 (ALDH3A1): Biochemical characterization and immunohistochemical localization in the cornea. *Biochem. J.* **376,** 615–623

36. Mitchell, J., and Cenedella, R. J. (1995) Quantitation of ultraviolet light-absorbing fractions of the cornea. *Cornea* **14,** 266–272

37. Bury, A. F. (1981) Analysis of protein and peptide mixtures. Evaluation of three sodium dodecyl sulfate-polyacrylamide gel electrophoresis buffer systems. *J. Chromatogr.* **213,** 491–500

38. Rabilloud, T., Adessi, C., Giraudel, A., and Lunardi, J. (1997) Improvement of the solubilization of proteins in two-dimensional electrophoresis with immobilized pH gradients. *Electrophoresis* **18,** 307–316

39. Herbert, B. (1999) Advances in protein solubilisation for two-dimensional electrophoresis. *Electrophoresis* **20,** 660–663

40. Görg, A., Obermaier, C., Boguth, G., Harder, A., Scheibe, B., Wildgruber, R., and Weiss, W. (2000) The current state of two-dimensional electrophoresis with immobilized pH gradients. *Electrophoresis* **21,** 1037–1053

41. Shevchenko, A., Wilm, M., Vorm, O., and Mann, M. (1996) Mass spectrometric sequencing of proteins silver-stained polyacrylamide gels. *Anal. Chem.* **68,** 850–858

42. Boeckmann, B., Bairoch, A., Apweiler, R., Blatter, M. C., Estreicher, A., Gasteiger, E., Martin, M. J., Michoud, K., O'Donovan, C., Phan, I., Pilbout, S., and Schneider, M. (2003) The SWISS-PROT protein knowledgebase and its supplement TrEMBL in 2003. *Nucleic Acids Res.* **31,** 365–370

43. Perkins, D. N., Pappin, D. J., Creasy, D. M., and Cottrell, J. S. (1999) Probability-based protein identification by searching sequence databases using mass spectrometry data. *Electrophoresis* **20,** 3551–3567

44. Jester, J. V., Barry, P. A., Lind, G. J., Petroll, W. M., Garana, R., and Cavanagh, H. D. (1994) Corneal keratocytes: In situ and in vitro organization of cytoskeletal contractile proteins. *Invest. Ophthalmol. Vis. Sci.* **35,** 730–743

45. Fini, E. M. (1999) Keratocyte and fibroblast phenotypes in the repairing cornea. *Prog. Retin. Eye Res.* **18,** 529–551

46. Piatigorsky, J. (2001) Enigma of the abundant water-soluble cytoplasmic proteins of the cornea: the "refracton" hypothesis. *Cornea* **20,** 853–858

47. Piatigorsky, J. (2000) Review: A case for corneal crystallins. *J. Ocul. Pharmacol. Ther.* **16,** 173–180

48. Boraldi, F., Bini, L., Liberatori, S., Armini, A., Pallini, V., Tiozzo, R., Ronchetti, I. P., and Quaglino, D. (2003) Normal human dermal fibroblasts: Proteomic analysis of cell layer and culture medium. *Electrophoresis* **24,** 1292–1310

49. Boraldi, F., Bini, L., Liberatori, S., Armini, A., Pallini, V., Tiozzo, R., Pasquali-Ronchetti, I., and Quaglino, D. (2003) Proteome analysis of dermal fibroblasts cultured in vitro from human healthy subjects of different ages. *Proteomics* **3,** 917–929

50. Celis, J. E., Dejgaard, K., Madsen, P., Leffers, H., Gesser, B., Honore, B., Rasmussen, H. H., Olsen, E., Lauridsen, J. B., Ratz, G., et al. (1990) The MRC-5 human embryonal lung fibroblast two-dimensional gel cellular protein database: Quantitative identification of polypeptides whose relative abundance differs between quiescent, proliferating and SV40 transformed cells. *Electrophoresis* **11,** 1072–1113

51. Stramer, B. M., Cook, J. R., Fini, M. E., Taylor, A., and Obin, M. (2001) Induction of the ubiquitin-proteasome pathway during the keratocyte transition to the repair fibroblast phenotype. *Invest. Ophthalmol. Vis. Sci.* **42,** 1698–1706

52. Feo, S., Arcuri, D., Piddini, E., Passantino, R., and Giallongo, A. (2000) ENO1 gene product binds to the c-myc promoter and acts as a transcriptional repressor: Relationship with Myc promoter-binding protein 1 (MBP-1). *FEBS Lett.* **473,** 47–52

53. Wallin, R., Hutson, S. M., Cain, D., Sweatt, A., and Sane, D. C. (2001) A molecular mechanism for genetic warfarin resistance in the rat. *FASEB J.* **15,** 2542–2544

54. Tulin, E. E., Onoda, N., Nakata, Y., Maeda, M., Hasegawa, M., Nomura, H.,

and Kitamura, T. (2001) SF20/IL-25, a novel bone marrow stroma-derived growth factor that binds to mouse thymic shared antigen-1 and supports lymphoid cell proliferation. *J. Immunol.* **167,** 6338–6347

55. Tulin, E. E., Onoda, N., Nakata, Y., Maeda, M., Hasegawa, M., Nomura, H., and Kitamura, T. (2003) Letter of Retraction: SF20/IL-25, a novel bone marrow stroma-derived growth factor that binds to mouse thymic shared antigen-1 and supports lymphoid cell proliferation. *J. Immunol.* **170,** 1593

56. Brissette-Storkus, C. S., Reynolds, S. M., Lepisto, A. J., and Hendricks, R. L. (2002) Identification of a novel macrophage population in the normal mouse corneal stroma. *Invest. Ophthalmol. Vis. Sci.* **43,** 2264–2271

57. Hamrah, P., Liu, Y., Zhang, Q., and Dana, M. R. (2003) The corneal stroma is endowed with a significant number of resident dendritic cells. *Invest. Ophthalmol. Vis. Sci.* **44,** 581–589

58. Berlett, B. S., and Stadtman, E. R. (1997) Protein oxidation in aging, disease, and oxidative stress. *J. Biol. Chem.* **272,** 20313–20316

59. Ghezzi, P., and Bonetto, V. (2003) Redox proteomics: Identification of oxidatively modified proteins. *Proteomics* **3,** 1145–1153

60. Lenaz, G. (1998) Role of mitochondria in oxidative stress and ageing. *Biochim. Biophys. Acta* **1366,** 53–67

61. Siegers, K., Bolter, B., Schwarz, J. P., Bottcher, U. M., Guha, S., and Hartl, F. U. (2003) TRiC/CCT cooperates with different upstream chaperones in the folding of distinct protein classes. *EMBO J.* **22,** 5230–5240

62. Grune, T., Merker, K., Sandig, G., and Davies, K. J. (2003) Selective degradation of oxidatively modified protein substrates by the proteasome. *Biochem. Biophys. Res. Commun.* **305,** 709–718

63. Giasson, B. I., Duda, J. E., Murray, I. V., Chen, Q., Souza, J. M., Hurtig, H. I., Ischiropoulos, H., Trojanowski, J. Q., and Lee, V. M. (2000) Oxidative damage linked to neurodegeneration by selective α-synuclein nitration in synucleinopathy lesions. *Science* **290,** 985–989

64. Lou, M. F. (2003) Redox regulation in the lens. *Prog. Retin. Eye Res.* **22,** 657–682